Received: 11 July 2022 | Revised: 21 December 2022 | Accepted: 2 March 2023

DOI: 10.1002/eqe.3873

RESEARCH ARTICLE

WILEY

Flexure-axial-shear interaction of ductile beams with single-crack plastic hinge behaviour

Eyitayo A. Opabola[1] | **Kenneth J. Elwood**[2]

[1]Department of Civil, Environmental and Geomatic Engineering, University College London, London, UK

[2]Department of Civil and Environmental Engineering, University of Auckland, Auckland, New Zealand

Correspondence
Eyitayo A. Opabola, Department of Civil, Environmental and Geomatic Engineering, University College London, London, UK.
Email: e.opabola@ucl.ac.uk

Funding information
QuakeCoRE NZ; UK Research and Innovation

Abstract

One of the key damage observations in modern reinforced concrete (RC) frame buildings, damaged following the 2010/2011 Canterbury and 2016 Kaikoura earthquakes, was localised cracking at the beam-column interface of capacity-designed beams. The localised cracking in the beams was due to curtailed longitudinal bars at the beam-column interface. Following these observations, without experimental data to justify desirable seismic performance, modern beams controlled by localised cracking were assumed to be potentially earthquake-vulnerable. To address this, an experimental program was carried out on six RC beam specimens susceptible to single-crack plastic hinge behaviour due to curtailed longitudinal bars. The experimental data show that RC beams with single-crack plastic hinge behaviour can undergo significant inelastic drift demands without loss of lateral resistance. However, contrary to conventional beams with distributed cracking, the response of RC beams with single-crack plastic hinge behaviour due to curtailed longitudinal bars is mainly dominated by hinge rotation (via bond-slip) and shear sliding at the column face. The current paper studies the interdependence of axial elongation, bond-slip and shear sliding deformation of RC beams with single-crack plastic hinge behaviour under cyclic demands. A procedure for seismic assessment of RC beams with single-crack plastic hinge behaviour due to curtailed longitudinal bars is proposed. The proposed formulations can be adopted to develop adequate numerical models for simulating the response of RC frames with beams susceptible to single-crack plastic hinge behaviour due to curtailed longitudinal bars.

KEYWORDS

axial elongation, deformation capacity, ductile beam, localised cracking, shear sliding, single-crack

1 | INTRODUCTION

Reconnaissance reports[1] following the 2010/2011 Canterbury and 2016 Kaikoura earthquakes highlighted various damage mechanisms in older-type and modern reinforced concrete (RC) frame structures. Aside from the well-known non-ductile behaviour of poorly-confined RC columns and walls, localised cracking was observed in various damaged RC structural

NOVELTY

Following the 2010/2011 Canterbury and 2016 Kaikoura earthquakes, a number of RC beams in high-rise structures exhibited localised cracking mechanism. The single crack response was due to longitudinal bar curtailment in the beams at the column face. There are currently no experimental data or assessment guidance on the seismic behaviour of these beams. However, it is now known that many existing frame buildings in New Zealand and United States have beams with curtailed bars.

To address this, this study:

- Presents experimental data on the seismic response of six full-scale beams susceptible to single crack response.
- Uses the experimental data to study and develop numerical formulations for predicting the interdependence of shear sliding deformation and axial elongation in such beams.
- Proposes a seismic assessment procedure for such beams.

components. The localised cracking in RC walls was attributed to the low longitudinal reinforcement in these walls, resulting in the cracking moment capacity being higher than the flexural strength of the walls.[2] In the case of modern RC moment frames with localised cracking at beam ends (See Figure 1A), the limited-crack mechanism was attributed to the common pre-castconstruction practice of bar curtailment close to the column face (Figure 1B). In the case of bar curtailment in beams close to the column face, the yield moment capacity of the beam section at the column face is significantly smaller than that of sections adjacent to the column face; resulting in a concentration of cracking at the column face.[3] It is noted that the bar curtailment detailing is also a common construction practice in the United States.[4]

Irrespective of building type or age, it was widely assumed that the localised cracking mechanisms in modern beams would potentially reduce the plastic rotation capacity of the hinges, premature rupture of the reinforcing bars, and lower hysteretic energy dissipation. Also, locally-concentrated strain in the bars may impact the residual low-cycle fatigue life available to withstand future earthquakes.[5] Hence, RC components determined to be susceptible to single-crack plastic hinge behaviour were assumed to be potentially earthquake-vulnerable.[6] In the case of modern RC beams with single-crack plastic hinge behaviour, such conservatism means that post-1995 capacity-designed buildings may be considered to require intervention.

Given the high cost associated with retrofitting buildings considered earthquake-vulnerable, there is a huge financial burden on building owners, the government, and the economy of countries with a high level of seismicity. To ease this burden, it is essential to develop refined seismic assessment provisions that will aid engineers in identifying the most vulnerable structures and prioritising them for the appropriate intervention strategies.

An experimental program on six full-scale beam specimens of a ten-story RC frame building in Wellington (designed in 1986) was developed to understand better the response of modern beams susceptible to single-crack plastic hinge behaviour. The aim of the study was to (a) understand the seismic response of beams susceptible to single-crack plastic hinge behaviour due to curtailed longitudinal bars; (b) understand the post-earthquake residual capacity and repairability of damaged beams susceptible to single-crack plastic hinge behaviour due to curtailed longitudinal bars; (c) develop

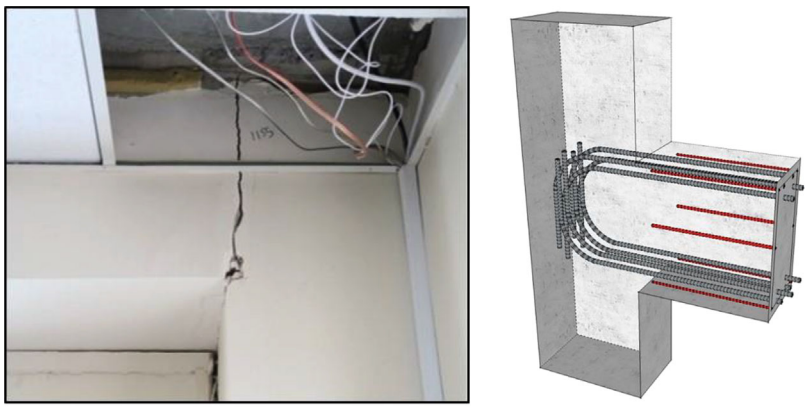

(A) (B)

FIGURE 1 (A) Observed damage following the 2016 Kaikoura earthquake (Photo by Synge A) (B) Bar curtailment detailing close to the column face (NB:—Curtailed bars are in red colour).

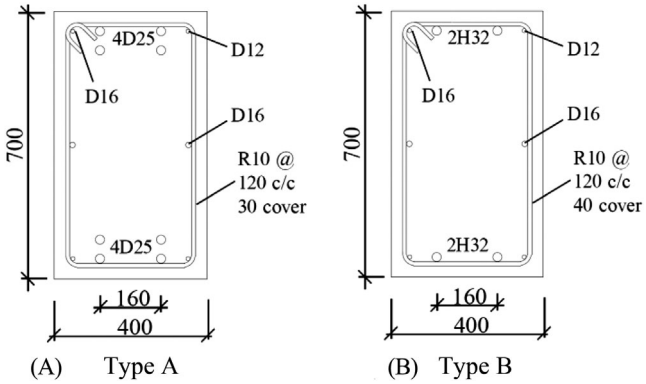

FIGURE 2 Cross-section of beam specimens (All D12 and D16 bars are curtailed as shown in Figure 1B).

formulations for predicting the seismic response of beams susceptible to single-crack plastic hinge behaviour due to curtailed longitudinal bars.

The experimental test data from these six beam specimens show that modern beams with single-crack plastic hinge behaviour due to curtailed longitudinal bars can withstand significant inelastic demands. However, the damage mechanism of the beams with single-crack plastic hinge behaviour due to curtailed longitudinal bars significantly influences the axial elongation-shear sliding relationship under drift demand; such that models developed for beams with distributed cracking may not be applicable for beams with single-crack plastic hinge behaviour. Without appropriate formulations to quantify the interdependence of shear sliding deformation and axial elongation of RC beams with a single-crack plastic hinge mechanism, numerical modelling of RC frame structures with these components becomes difficult. Hence, it is important to understand the flexure-axial elongation-shear sliding relationship of RC beams with a single-crack plastic hinge mechanism.

Using measured data from the six beam specimens, this paper seeks to develop numerical formulations for the seismic behaviour of beams with a single-crack plastic hinge behaviour. The interdependence of shear sliding deformation and axial elongation was studied. Subsequently, simple formulations are proposed to simulate the interdependence of shear sliding deformation and axial elongation. Also, a seismic assessment procedure for such beams is proposed. The proposed formulations can be adopted in developing adequate numerical models for simulating the response of RC frames with beams susceptible to single-crack plastic hinge behaviour.

2 | EXPERIMENTAL PROGRAM

An experimental program was carried out on six full-scale replica beams with bar curtailment detailing similar to those in a ten-storey ductile RC frame building with localised beam hinging following the 2016 Kaikoura earthquake. All six beam specimens have a 400 mm × 700 mm cross-section dimension (Figure 2). The frame building, situated on a site class C soil in Wellington, was designed in accordance to NZS 3101:1982.[7] It is noted that the provided transverse and main longitudinal reinforcement detailing conform to NZS 3101:2006.A3 provisions.[8]

Four of the beams (CYC-1.96.25, EQ-R-1.96.25, EQ-S-1.96.25, and EQ-D-1.96.25) are nominally identical specimens with a shear span of 1960 mm (Table 1). Different displacement histories were adopted for these four specimens. Specimen CYC-1.96.25, the baseline specimen, was subjected to a standard cyclic loading protocol (Figure 3A). EQ-R-1.96.25 was used to assess the reparability of beams susceptible to single-crack plastic hinge behaviour. Following an initial earthquake (EQ) protocol (Part I) with a peak drift of 1%, the beam was repaired using epoxy injection before being subjected to another EQ protocol with a peak drift of 2%, followed by one loading cycle at 3% drift (Part II) (See Figure 3B). The EQ protocol was derived from a time-history analysis of a structural model of the ten-storey building using a 2016 Kaikoura ground motion record from a nearby station. Further discussions on the building model are available in Opabola and Elwood.[3]

With the aim of studying the residual capacity of damaged beams, specimen EQ-S-1.96.25 was initially subjected to an earthquake (EQ) loading history with a peak drift of 3%, followed by a standard cyclic loading protocol (See Figure 3C). It is noted that the EQ loading protocol for EQ-S-1.96.25 was applied at a static loading rate of 0.75 mm/s (Table 1). EQ-D-1.96.25 was subjected to a similar loading history as EQ-S-1.96.25, except that the EQ loading history was applied at a dynamic rate of 75 mm/s. EQ-S-1.96.25 and EQ-D-1.96.25 provided an avenue to understand the influence of loading rate on the behaviour of pristine beams and the residual capacity of damaged beams.

TABLE 1 Test matrix.

Specimen ID[a]	Cross-section type	Aspect ratio (a/d)	Bar size d_b (mm)	Steel grade (MPa)	Test type
CYC-1.96.25	A	3.2	25	300	Quasi-static cyclic (0.75 mm/s)
CYC-1.24.25	A	2.0	25	300	Quasi-static cyclic (0.75 mm/s)
CYC-1.96.32	B	3.2	32	500	Quasi-static cyclic (0.75 mm/s)
EQ-S-1.96.25	A	3.2	25	300	Quasi-static EQ (0.75 mm/s) + Quasi-static cyclic (0.75 mm/s)
EQ-D-1.96.25	A	3.2	25	300	Pseudo-dynamic EQ (75 mm/s) + Quasi-static cyclic (0.75 mm/s)
EQ-R-1.96.25	A	3.2	25	300	Quasi-static EQ + repair + Quasi-static EQ + 1 cycle at 3% drift (Reparability test)

[a]Specimen ID labels is related to the shear span (1.96 m or 1.24 m), bar size (25 mm or 32 mm) and loading protocol adopted in the specimens. CYC—Cyclic; EQ—Earthquake protocol; S—Quasi-static; D—Pseudo-dynamic; R—Repaired.

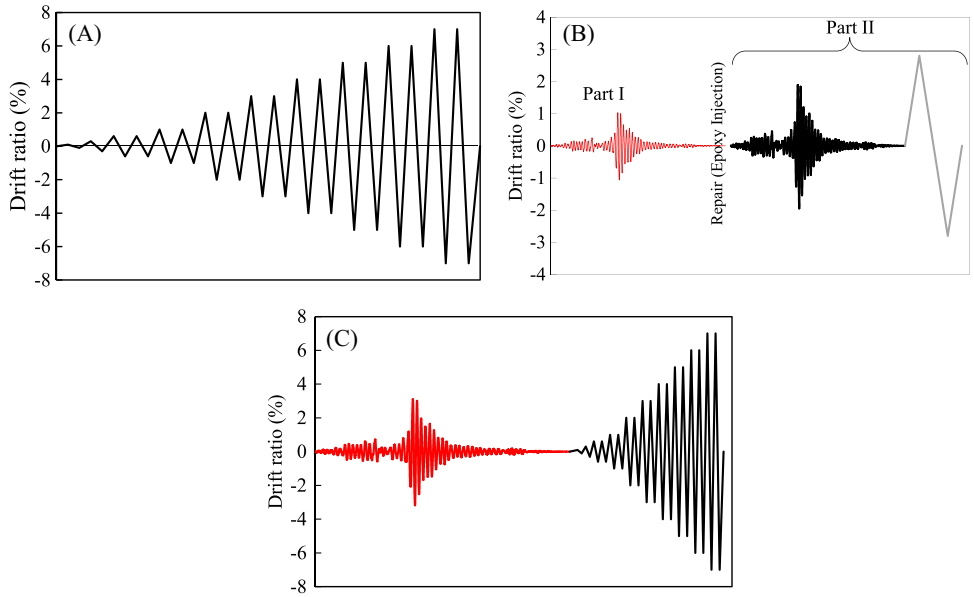

FIGURE 3 Loading protocol for test specimens.

Specimen CYC-1.24.25 has cross-section properties similar to CYC-1.96.25. However, the shear span was reduced to 1240 mm to study the influence of high shear stress on the damage mechanism of beams susceptible to single-crack plastic hinge behaviour. Specimen CYC-1.96.32 has a shear span of 1960 mm, but the longitudinal reinforcement diameter was increased to 32 mm (Figure 2B). CYC-1.96.32 was used to study the influence of larger bar size and higher steel grade on the behaviour of beams susceptible to single-crack plastic hinge behaviour. Both CYC-1.24.25 and CYC-1.96.32 were subjected to the standard cyclic loading protocol. For the sake of brevity, discussions on instrumentation layout are not presented here. Interested readers are referred to Opabola and Elwood.[3]

3 | EXPERIMENTAL RESULTS

3.1 | Damage pattern and deformation component hysteretic behaviour

The observed damage patterns in specimens CYC-1.96.25, CYC-1.24.25, and CYC-1.96.32 are presented in Figure 4. As shown in Figure 4A, the response of CYC-1.96.25 was dominated by the single crack at the beam end. Secondary cracks with maximum crack width less than 0.25 mm formed away from the specimen end during the elastic phase. However, none of these secondary cracks had any significant progression during the inelastic phase. A similar pattern

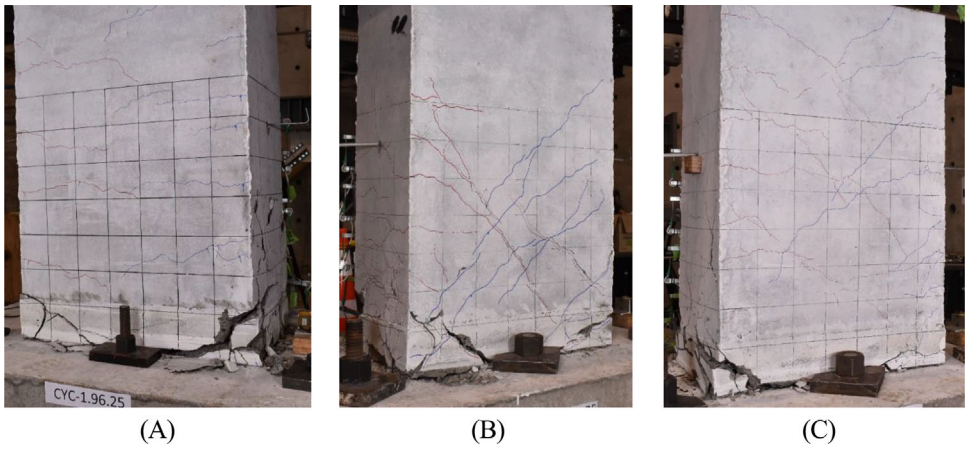

FIGURE 4 Damage pattern of (A) CYC-1.96.25 (B) CYC-1.24.25 (C) CYC-1.96.32 at 3% drift.

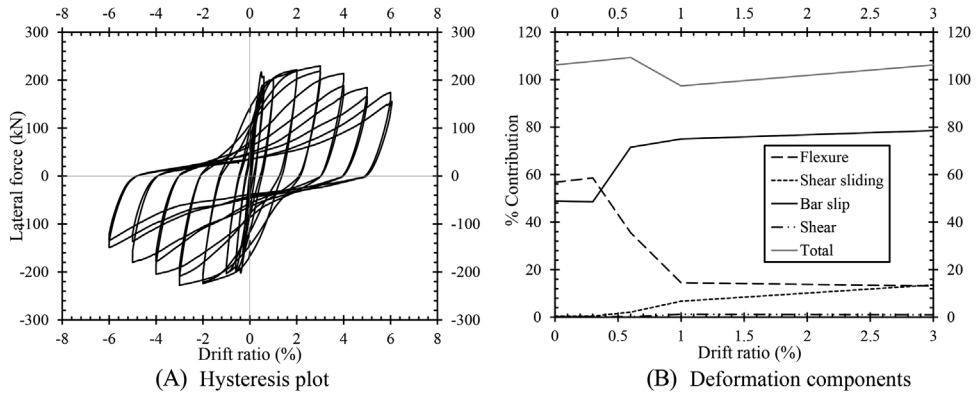

FIGURE 5 (A) Hysteresis plot and (B) contribution of deformation components to response of specimen CYC-1.96.25.

was observed in specimens EQ-S-1.96.25, EQ-D-1.96.25, and EQ-R-1.96.25. The hysteresis plot for CYC-1.96.25 is shown in Figure 5A. As shown in Figure 5A, CYC-1.96.25 was able to withstand significant drift demands before the onset of lateral strength loss. Using data from instrumentation, Figure 5B shows the contribution of various deformation components to the total response of CYC-1.96.25. As shown in Figure 5B, prior to flexural yielding of CYC-1.96.25, bond-slip deformation contributes about 48% of the total deformation, but this increases to about 80% in the post-yield phase. There is also an increase in shear sliding with increasing drift demands, attributed to axial elongation concentrated at the beam-foundation interface, leading to a reduction in aggregate interlock resistance.

The higher shear distress in CYC-1.24.25 resulted in a switch to a flexure-shear mechanism with significant diagonal cracking observed (Figure 4B). This observation agrees with previous conclusions[9] that beams with shear stress $\geq 0.25\sqrt{f'_c}$ (MPa) are likely to have a higher contribution of shear deformation. On the other hand, the damage pattern of CYC-1.96.32 was similar to CYC-1.96.25 until a drift demand of 3%. Afterwards, longitudinal cracks (attributed to the dowel action in the tensile bars) formed in the specimen. The force-displacement and deformation components for CYC-1.24.25, and CYC-1.96.32 are not presented here. Interested readers are referred to Opabola and Elwood.[3] However, Table 2 shows that both beams were able to sustain significant drift demands before the onset of lateral strength loss. It is noted that bar fracture was not observed in any of the test specimens. However, significant buckling of the longitudinal bars was observed in all specimens. Further information on the damage mechanisms, hysteretic response, deformation components, residual capacity and reparability of the test specimens can be found in Opabola.[3] In agreement with the aim of this study, subsequent sections will focus on understanding and proposing formulations for modelling the interdependence of shear sliding deformation and axial elongation in beams susceptible to single-crack plastic hinge behaviour.

TABLE 2 Measured force-drift parameters for all test beams.

Specimen		Peak strength V_{max} (kN)		$V_{max}/(bd\sqrt{f'_c})$ (MPa)	Measured θ_y (%)[a]	Effective stiffness (EI_{eff}/EI_g)	Measured θ_u (%)[b]
		(+)	(−)				
CYC-1.96.25		229.9	227.6	0.17	0.48	0.22	5.0
CYC-1.24.25		346.4	350.7	0.26	0.4	0.16	5.0
CYC-1.96.32		299	299.3	0.22	0.8	0.2	7.0
EQ-S-1.96.25	EQ	233.5	233.2	0.17	0.6	0.18	–
	CYC	202	202.2	0.15	–	0.04	4.5
EQ-D-1.96.25	EQ	248.4	250.3	0.18	0.4	0.29	–
	CYC	186.2	189.9	0.14	–	0.046	4.5
EQ-R-1.96.25	Part I	203.7	216.2	0.16	0.38	0.25	–
	Part II	229.3	236.1	0.17	–	0.165	–

[a]The yield rotation (θ_y) is measured by drawing a secant line to pass through $0.7V_{max}$. The drift where the secant line intersects with the horizontal line drawn along V_{max} is taken as θ_y.
[b]The ultimate rotation (θ_u) is defined as the rotation corresponding to 20% loss in lateral strength.

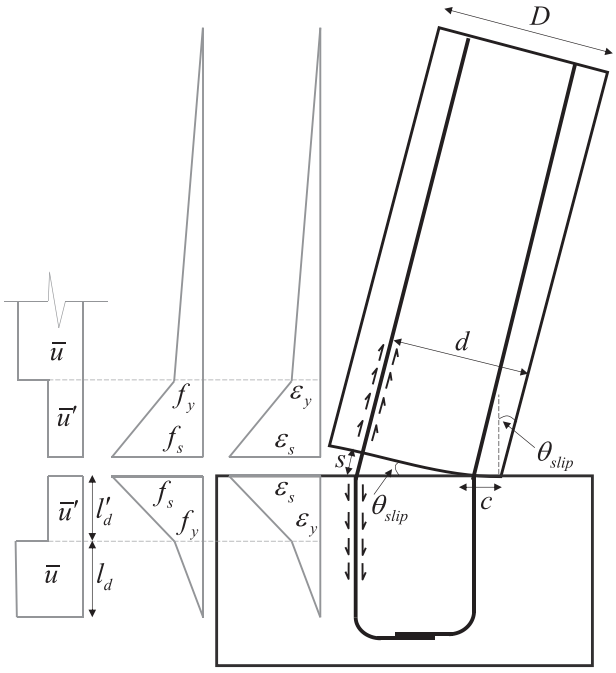

FIGURE 6 Stress-strain state of a RC component with a single-crack plastic hinge behaviour, assuming no shear sliding.

4 | RELATIONSHIP BETWEEN PURE BOND-SLIP AND DRIFT DEMAND

The stress-strain state of tensile bars in the anchorage and shear span of a RC component, assuming pure bond-slip behaviour, is represented in Figure 6. The slip at the end-section can be estimated by integrating the strain in the reinforcing bar along the development length such that:

$$s = \int_0^{l_d + l_d'} \varepsilon_s(x)\, dx \tag{1}$$

where l_d and l_d' are the development lengths for the elastic and inelastic portions of the bar, respectively.

Assuming a uniform bond stress, an expression for the development length in the elastic portion of the bar is given by:

$$l_d = \frac{f_s d_b}{4\bar{u}} \tag{2}$$

Where $\bar{u}$ is the elastic bond stress, d_b is the longitudinal reinforcement diameter and f_s is the stress in the reinforcement.

By adopting a linear strain-hardening law, the post-yield steel stress f_s can be evaluated as a function of the steel strain ε_s, yield steel stress f_y and strain ε_y; ultimate steel stress f_u and strain ε_u such that:

$$f_s = f_y + \left(f_u - f_y\right)\frac{\left(\varepsilon_s - \varepsilon_y\right)}{\left(\varepsilon_u - \varepsilon_y\right)} \tag{3}$$

The development length in the inelastic portion of the reinforcing bar can be estimated as:

$$l_d{}' = \frac{\left(f_s - f_y\right)d_b}{4\bar{u}'} = \frac{d_b\left(f_u - f_y\right)}{4\bar{u}'}\frac{\left(\varepsilon_s - \varepsilon_y\right)}{\left(\varepsilon_u - \varepsilon_y\right)} \tag{4}$$

where $\bar{u}'$ is the inelastic bond stress and can be taken as $0.5\sqrt{f_c'}$ in MPa units.[10]

For a linear strain distribution, the reinforcement slip during the inelastic phase, s_p*, can be estimated by solving Equation (1) such that:

$$s_p^* = \frac{\varepsilon_s + \varepsilon_y}{2} l_d{}' = \frac{d_b\left(f_u - f_y\right)}{8\bar{u}'}\frac{\left(\varepsilon_s + \varepsilon_y\right)}{\left(\varepsilon_u - \varepsilon_y\right)}\left(\varepsilon_s - \varepsilon_y\right) \tag{5}$$

Equation (5) is the inelastic reinforcement slip due to strain penetration into just one side of the principal crack. As shown in Figure 6, however, there is strain penetration on both sides of the principal crack. Hence, the inelastic reinforcement slip due to strain penetration into both sides of the crack (s_p) can be taken as:

$$s_p = 2s_p^* = \frac{d_b\left(f_u - f_y\right)}{4\bar{u}'}\frac{\left(\varepsilon_s + \varepsilon_y\right)}{\left(\varepsilon_u - \varepsilon_y\right)}\left(\varepsilon_s - \varepsilon_y\right) \tag{6}$$

The plastic rotation of the beam is given as:

$$\theta_p = \frac{s_p}{d - c} = \frac{d_b\left(f_u - f_y\right)}{4\bar{u}'}\frac{\left(\varepsilon_s + \varepsilon_y\right)}{\left(\varepsilon_u - \varepsilon_y\right)}\frac{\left(\varepsilon_s - \varepsilon_y\right)}{(d - c)} \tag{7}$$

It is noteworthy that if ε_s equals ε_u and it is assumed that the change in compression zone depth c between the yield state and ultimate state is negligible, then

$$\frac{\left(\varepsilon_s - \varepsilon_y\right)}{(d - c)} = \frac{\left(\varepsilon_u - \varepsilon_y\right)}{(d - c)} \approx \phi_u - \phi_y = \phi_p \tag{8}$$

According to Paulay and Priestley,[11] the plastic rotation of a beam can be expressed as a function of the plastic curvature ϕ_p and plastic hinge length L_p, such that

$$\theta_p = \left(\phi_u - \phi_y\right)L_P = \phi_p L_p \tag{9}$$

Assuming the plastic hinge length L_p equals the strain penetration length into both sides of the crack ($2l_{sp}$) and putting Equation (8) into Equation (7) and equating this to Equation (9), the strain penetration depth equals

$$l_{sp} = \frac{d_b\left(f_u - f_y\right)}{8\bar{u}'}\frac{\left(\varepsilon_s + \varepsilon_y\right)}{\left(\varepsilon_u - \varepsilon_y\right)} \tag{10}$$

At ultimate state, ε_s equals ε_u and by assuming $\varepsilon_u >> \varepsilon_y$ and $\bar{u}'$ equals $0.5\sqrt{f'_c}$ in MPa units, strain penetration length can be evaluated as:

$$l_{sp} = \frac{d_b\left(f_u - f_y\right)}{8\bar{u}'} = \frac{\left(\frac{f_u}{f_y} - 1\right) f_y d_b}{4\sqrt{f'_c}} \tag{11}$$

For range of f_u/f_y between 1.2 and 1.5,[12] the value of l_{sp} ranges from 0.008 to 0.025. For f_u/f_y equals 1.5, a concrete compressive strength (f'_c) of 30 MPa, Equation (11) would yield a strain penetration value of l_{sp} equals $0.023 f_y d_b$. It is noteworthy that Paulay and Priestley[11] had previously proposed that l_{sp} equals $0.022 f_y d_b$.

Based on the previous assumption that ε_s equals ε_u and $\varepsilon_u >> \varepsilon_y$, the plastic rotation due to strain penetration in both directions can be estimated by putting Equation (10) into Equation (7):

$$\theta_p = \frac{2s_p}{d-c} = \frac{2\varepsilon_s l_{sp}}{(d-c)} \tag{12}$$

Equation (12) can be combined with Equation (11) to give Equation (13).

$$\theta_p = \frac{\varepsilon_s}{(d-c)} \frac{\left(\frac{f_u}{f_y} - 1\right) f_y d_b}{2\sqrt{f'_c}} \tag{13}$$

Equation (13) provides an estimate of the plastic rotation capacity, given an ultimate strain capacity of the longitudinal reinforcement, of a beam dominated by a pure bond-slip mechanism. Given that the response of beams with single-crack plastic hinge behaviour is not dominated by a pure bond-slip mechanism, additional measures may be required to account for the contribution of shear sliding deformation. Hence, it is important to explore formulations to predict the relationship between axial elongation and shear sliding in beams with single-crack plastic hinge behaviour under drift demand. Such formulations are described subsequently in this paper.

5 | RELATIONSHIP BETWEEN AXIAL ELONGATION AND DRIFT DEMAND

The relationship between axial elongation and drift ratio for all six specimens is presented in Figure 7. Experimental data suggest that, for the same drift demand, CYC-1.96.32 had more significant axial elongation than CYC-1.96.25 (See Figure 7). This can be attributed to the influence of larger bar size and higher steel grade on strain penetration in CYC-1.96.32. It is also noted that experimental data from tests on undamaged specimens EQ-S-1.96.25 and EQ-D-1.96.25 do not suggest a strong influence of loading rate on axial elongation.

Researchers such as Fenwick and Megget[13] have studied the axial elongation response of beams with distributed cracking. Axial elongation is associated with the residual strains in the compression and tension reinforcement under cyclic reversals. Plasticity spread in beams with distributed cracking is primarily due to flexural curvature and bond slip. In beams with single-crack plastic hinge behaviour, the spread of inelasticity is mainly due to bond slip. Hence, it is important to explore the axial elongation—drift demand relationship in cases where localised cracking is expected.

Figure 8 represents the response of a single-curvature beam with single-crack plastic hinge behaviour undergoing cyclic actions at a displacement demand Δ. Under this displacement demand, the concentration of damage at the beam-column interface results in crack widths of δ_1 and δ_2 at the location of the tension and compression bars, respectively. The crack width at the location of the compression bar δ_2 is attributed to the influence of irreversible extensions of the compression reinforcement. Under larger displacement reversals, there is an irreversible extension of the compression reinforcement. This is due to insufficient compressive stress to yield the bars back in compression after they have previously yielded in tension, arising majorly from wedging action of the aggregates.[13] In Figure 8, the fixed-end rotation (θ_{slip}) is assumed to be equal to the total drift demand (θ_m) on the beam such that:

$$\theta_m = \frac{\Delta}{a} = \theta_{slip} = \frac{\delta_1 - \delta_2}{d - d'} \tag{14}$$

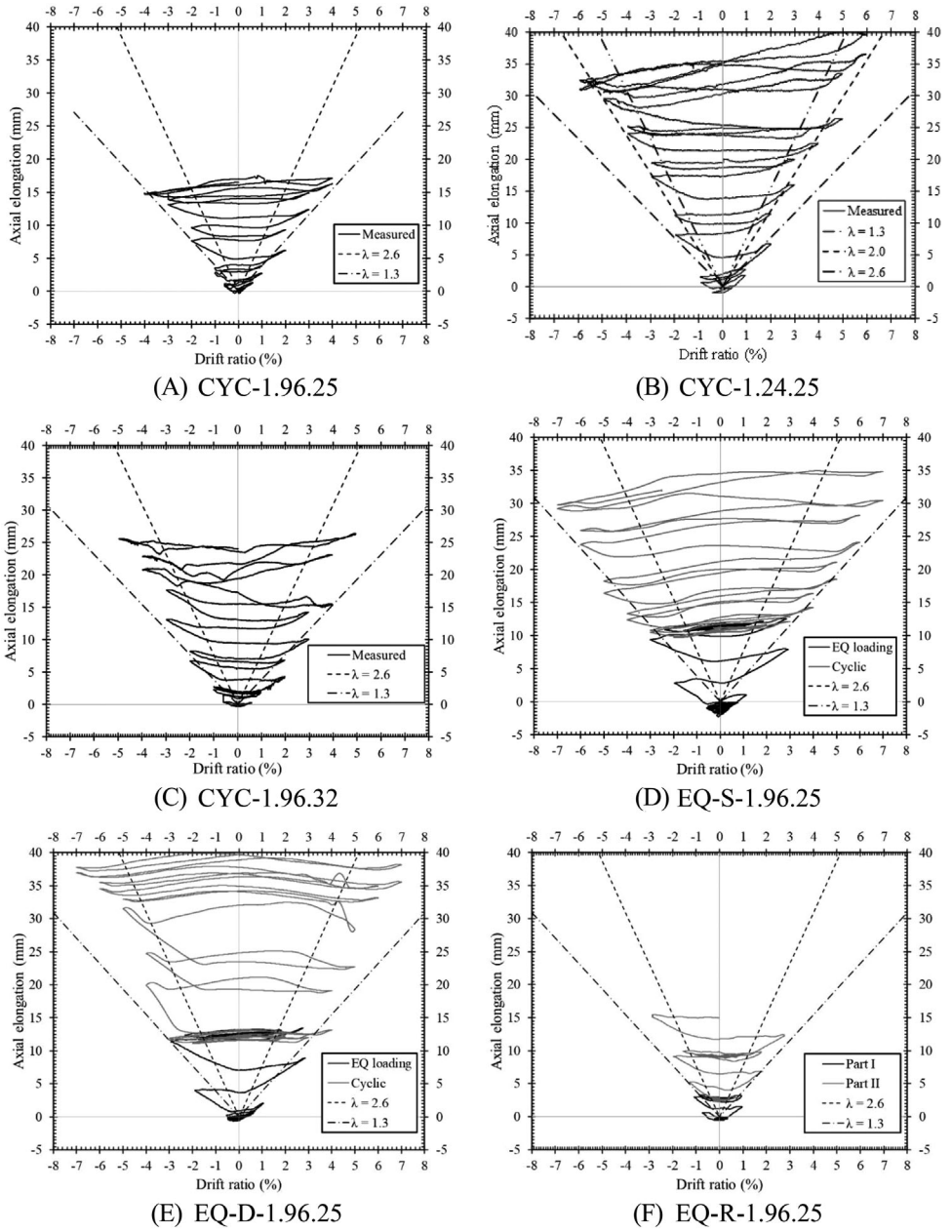

FIGURE 7 Relationship between axial elongation and drift ratio.

Likewise, the axial elongation of the beam is taken to be:

$$\delta_{el} = \frac{\delta_1 + \delta_2}{2} \tag{15}$$

Combining Equations (14) and (15), the axial elongation of the beam is evaluated as:

$$\delta_{el} = \delta_2 + \frac{\theta_m}{2}\left(d - d'\right) \tag{16}$$

If δ_2 is assumed to be dependent on drift demand, then:

$$\delta_{el} = \lambda\frac{\theta_m}{2}\left(d - d'\right) \tag{17}$$

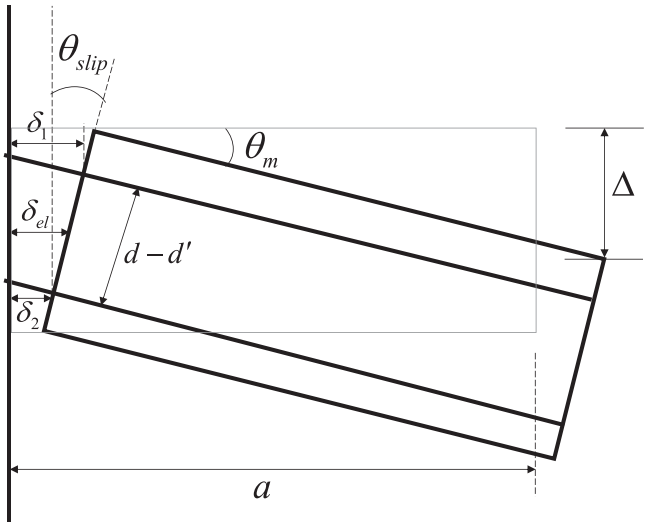

FIGURE 8 Axial elongation in a beam with single-crack plastic hinge mechanism.

Where λ is a coefficient accounting for the influence of irreversible extension of the compression reinforcement on beam elongation.

For a beam with single-crack plastic hinge behaviour under monotonic loading or low cyclic deformation demands, δ_2 will be close to zero, making λ equals unity and the elongation of the beam can be readily computed as:

$$\delta_{el} = \frac{\theta_m}{2}\left(d - d'\right) \tag{18}$$

It is noteworthy than Equation (18) has previously been verified by Fenwick and Megget[13] for components with distributed cracking.

Measured axial elongation in the beam specimens were compared with estimates using an axial elongation model, incorporated in NZS 3101:2006[8] for estimating axial elongation in beams with distributed cracking. According to NZS 3101:2006, axial elongation (δ_{el}) of a beam-column component with reversing plastic hinges can be estimated as:

$$\delta_{el} = 2.6\frac{\theta_m}{2}\left(d - d'\right) \tag{19}$$

A simple data fitting approach suggested that a value of λ of 1.3 (half of that proposed for beams with distributed cracking) is appropriate for Specimens CYC-1.96.25, CYC-1.96.32, EQ-S-1.96.25 and EQ-R-1.96.25 (See Figure 7). On the other hand, a λ value of 1.3 underestimates the cyclic test on EQ-D-1.96.25, despite providing a good estimate of the beam response during the EQ protocol. This suggests that the strain rate effect from a previous seismic event may have an influence on the axial elongation response of a damaged beam. Additional test data are, however, needed to further explore this.

Based on current data, for slender beams expected to be dominated by a single-crack plastic hinge behaviour,

$$\delta_{el} = 1.3\frac{\theta_m}{2}\left(d - d'\right) \tag{20}$$

As shown in Figure 7B, Equation (20) underestimates the response of the beam. This is not surprising, given the fact that the behaviour of Specimen CYC-1.24.25 was dominated by distributed cracking. Figure 7B also shows that Equation (19) slightly overestimates the response of Specimen CYC-1.24.25. A better relationship is estimated by assuming a $\lambda = 2.0$, which roughly coincides with the mid-way between $\lambda = 1.3$ and $\lambda = 2.6$. Hence, it is proposed that for beams with curtailed bars having $a/d \leq 2$ or $V_u/(bd\sqrt{f'_c}) \geq 0.25\sqrt{f'_c}$, Equation (17) should be adopted with $\lambda = 2.0$. Additional experimental data are required to validate this. If a high level of conservatism is required, however, a λ value of 2.6 may be adopted.

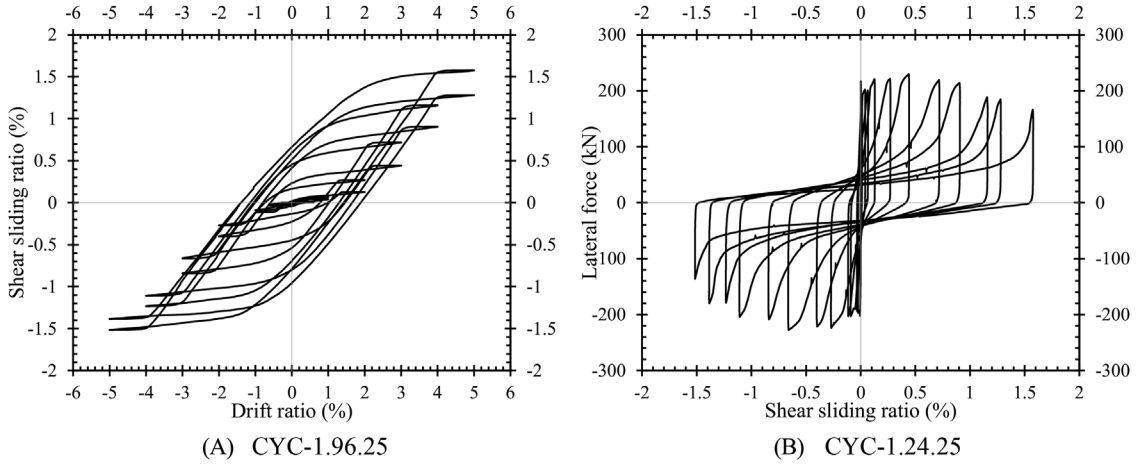

FIGURE 9 Lateral force versus shear sliding for specimens (A) CYC-1.96.25 (B) CYC-1.24.25.

6 | SHEAR SLIDING DEFORMATION AT BEAM-COLUMN INTERFACE

6.1 | Degradation of shear sliding stiffness with ductility

The contribution of shear sliding to the response of beams with a single-crack plastic hinge behaviour is quite significant. As seismic demand increases, the contribution of shear sliding increases as well. Figure 9A shows the relationship between drift ratio and shear sliding ratio (defined as the ratio of measured shear sliding displacement to beam shear span) for specimen CYC-1.96.25. The increase in shear sliding is attributed to the degradation of the shear transfer mechanism along the beam-column interface. The degradation of the shear transfer mechanism is majorly due to an increase in base crack width, leading to loss of aggregate interlock, degradation of dowel capacity of the longitudinal bars, and loss of concrete cover and confinement provided by stirrups. Experimental observations show that the stirrups are exposed to significant lateral pressure from the longitudinal bars under dowel action, leading to excessive buckling of these stirrups. Without this restraint, the resistance to sliding shear reduces.

Figure 9B shows the relationship between lateral shear resistance and shear sliding deformation for specimen CYC-1.96.25. As shown in Figure 9, there is a significant pinching behaviour after the beam has been subjected to drift demands. Two mechanisms contribute to the lateral stiffness provided by the longitudinal bars—the bearing of the bars on the concrete core and the bearing of the bars on the stirrups. During reversal from a peak drift, once no support is provided to the bars by the concrete core and stirrups, the shear sliding stiffness reduces significantly.

For the three specimens subjected to the standard cyclic protocol (i.e. specimens CYC-1.96.25, CYC-1.96.32 and CYC-1.24.25), the average shear sliding stiffness for the second cycle to each drift level was evaluated. The adopted approach is similar to that used in evaluating the lateral stiffness of the beams in a previous section. Shear sliding stiffness is evaluated as:

$$K_s = \frac{V^+ + |V^-|}{\Delta_{ss}^+ + |\Delta_{ss}^-|} \tag{21}$$

where V^+ and V^- are the peak positive and negative shear forces at the second cycle at a peak drift level respectively. Δ^+_{ss} and Δ^-_{ss} are the shear sliding displacements corresponding to these peak shear forces.

Each computed shear sliding stiffness is normalised against the shear sliding stiffness corresponding to the measured yield rotation of the specimen ($K_{s,y}$). Two relationships were explored—(a) the degradation of shear sliding stiffness relative to ductility demands (μ) (Figure 10A) and (b) the degradation of shear sliding stiffness relative to μ_s which is equal to $\Delta_{ss}/\Delta_{ss,y}$ (where $\Delta_{ss,y}$ is the shear sliding displacement at yield) (Figure 10B).

As shown in Figure 10, the relationship between shear sliding stiffness and μ (as well as μ_s) is nonlinear. The relationships can be expressed as:

$$\frac{K_s}{K_{s,y}} = \frac{1}{a_1 \mu^{a_2}} \tag{22}$$

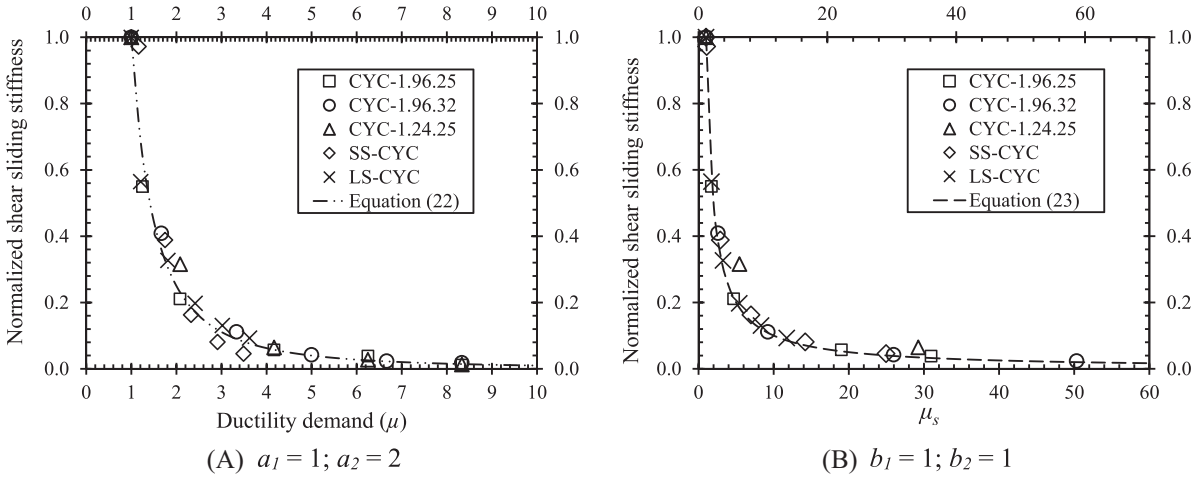

FIGURE 10 Relationship between sliding shear stiffness degradation, μ and μ_s for beams with single-crack and distributed crack response.

and

$$\frac{K_s}{K_{s,y}} = \frac{1}{b_1 \mu_s^{b_2}} \tag{23}$$

where a_1, a_2, b_1 and b_2 are coefficients relating shear sliding stiffness to μ and μ_s

Based on currently available data, Figure 10A shows that the relationship between shear stiffness degradation and ductility demand is best estimated using a_1 equals unity and a_2 equals 2. Likewise, the relationship between shear stiffness degradation and μ_s is best estimated using b_1 equals unity and b_2 equals unity (Figure 10B).

The relationship between shear stiffness degradation and μ_s can be mathematically proven by assuming a bilinear relationship between stiffness degradation and μ_s such that:

$$\frac{K_s}{K_{s,y}} = \frac{V_{\max}/\Delta_{ss}}{V_{\max}/\Delta_{ss,y}} = \frac{1}{\mu_s} \tag{24}$$

By combining Equations (22) and (24), the relationship between μ and μ_s can be determined; such that:

$$\mu_s = a_1 \mu^{a_2} \tag{25}$$

The relationship between μ and μ_s is plotted in Figure 11. As previously suggested, adopting an a_1 value of unity and a_2 value of 2 in Equation (25) provides a good estimate of the relationship between μ and μ_s for specimens CYC-1.96.25 and CYC-1.96.32. On the other hand, an a_2 value of 2.25 provides a better estimate for specimen CYC-1.24.25; suggesting that a_2 is dependent on aspect ratio, that is shorter beams are more susceptible to a significant increase in shear sliding displacement with an increase in ductility demands. Further testing is needed to validate this.

The applicability of Equations (22), (23) and (25) to conventionally reinforced beams with distributed cracking was explored. Sarrafzadeh[14] subjected two ductile beam specimens LS-CYC and SS-CYC, with aspect ratios of 3.4 and 2.8, respectively, to a standard cyclic protocol. As shown in Figures 10 and 11, the proposed relationships between shear sliding stiffness, μ and μ_s may be valid for beams with single-crack and distributed crack plastic hinge behaviour. However, it is noted that the relationship was only calibrated to data up until a ductility of about four for specimens SS-CYC and LS-CYC. Hence, care must be taken when using the model at larger ductility demands in beams with distributed cracking. Based on available data, the response of the shorter beam SS-CYC can be predicted by a_2 value of 2.25 while an a_2 value of 2 provides a good estimate for Specimen LS-CYC. Additional test data are needed to validate these conclusions.

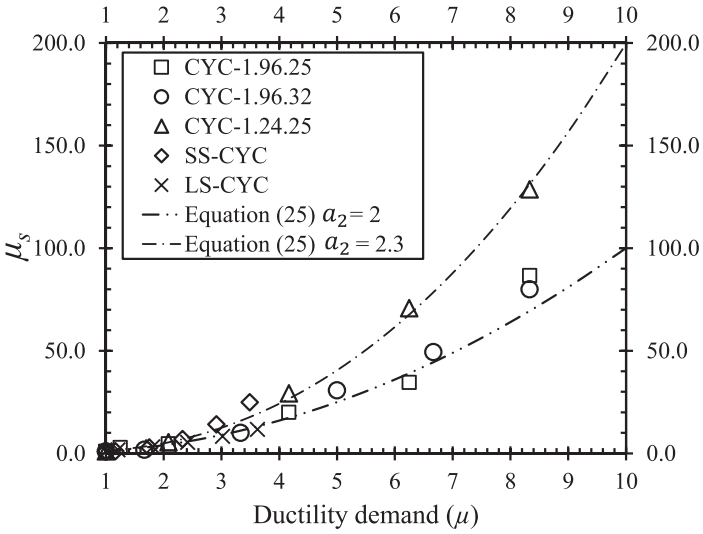

FIGURE 11 Relationship between μ and μ_s for beams with single-crack and distributed crack response.

Hence, it is proposed that for beams with single-crack and distributed crack response, a_2 equals 2 for beams with $a/d \geq 3$ and 2.25 for beams with $a/d < 3$. The values of a_1, b_1 and b_2 equal unity for all beams. Additional test data (including tests on restrained beams) are, however, needed to further validate the proposed expressions in this section.

For seismic assessment purposes, the shear sliding at a given ductility demand ($\mu = \theta_m/\theta_y$) can be derived from Equation (25) such that:

$$\Delta_{ss} = \left(\Delta_{ss,y}\right) \mu^{a_2} \tag{26}$$

In order to adopt Equation (26), it is important to evaluate the shear sliding displacement corresponding to the yield rotation of the beam ($\Delta_{ss,y}$). Discussions on the estimation of $\Delta_{ss,y}$ is provided below.

6.2 | Shear sliding during elastic response

Shear deformation in RC members is due to the combined effect of shear sliding at the beam-column interface, rigid shear distortion of member and shear sliding along diagonal cracks (more pronounced in squat members). Rather than derive complex formulations for evaluating shear sliding deformation at yield due to shear sliding at beam-column interface, it is proposed that evaluating shear sliding (at beam-column interface) deformation at yield be conservatively assessed as total shear deformation. Recall for a single-curvature beam, the shear sliding at yield can be computed as[15]:

$$\Delta_{ss,y} = \frac{M_{\max}}{A_v G_{eff}} \tag{27}$$

M_{max} is the moment corresponding to peak lateral resistance, A_v is the effective shear area, and it is equal to 5/6 of the gross cross-sectional area, and G_{eff} is adapted to be equal to $0.2E_c$.[15]

The adequacy of Equation (27), for all five specimens presented in Figure 10, is shown in Figure 12. As shown in Figure 12, Equation (27) provides good estimates of shear sliding displacement at yield for all specimens, except CYC-1.24.25 (shortest beam specimen) which was underestimated. This underestimation may be attributed to the fact that other forms of shear deformation (i.e. rigid shear distortion of member and shear sliding along diagonal cracks) also provide significant contributions to the total shear deformation of the beam. In slender beams, the contribution of shear distortion is relatively low, and no diagonal crack planes are formed; hence, it can be assumed that all shear deformation is provided by shear sliding displacement. Additional data are needed to provide a refined formulation for shear sliding displacement for squat beams. In the absence of such data, the adoption of Equation (27) is suggested.

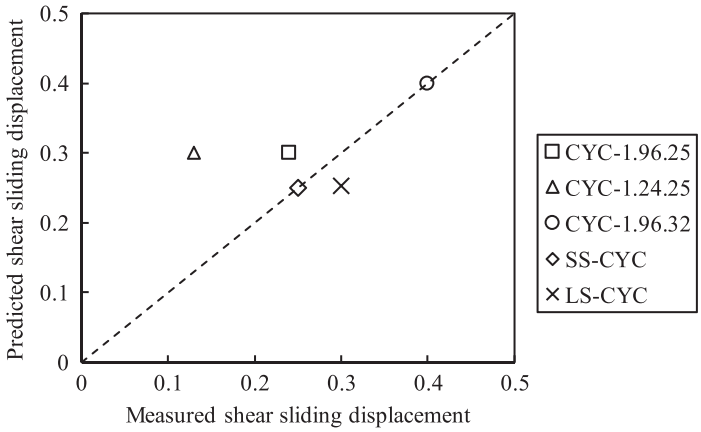

FIGURE 12 Prediction of shear sliding displacement at yield using Equation (27).

7 | MATHEMATICAL RELATIONSHIP BETWEEN SHEAR SLIDING AND AXIAL ELONGATION

Figure 13 shows the relationship between axial elongation and shear sliding for all beam specimens. As shown in the Figure, when the axial deformation in the beam is small, shear sliding deformation is not significant. As the beam continues to elongate under cyclic demands, the influence of cyclic action-induced shear-friction deterioration, separation of the two concrete interfaces, and excessive longitudinal bar buckling lead to a significant increase in shear sliding with a minimal increase in drift demand.

For specimen CYC-1.24.25 with a shear span of 1240 mm and aspect ratio of 2, due to diagonal cracking, shear deformation is split between sliding at the beam-column interface and sliding through the diagonal crack planes along the beam length. The reduced shear sliding at the beam-column interface suggests that the section of the longitudinal bars at the beam-column interface is subjected to lesser dowel action compared to other specimens with a shear span of 1960 mm and aspect ratio of 3.2.

As shown in Figure 13 the relationship between axial elongation and shear sliding is nonlinear. It is intuitive to expect that shear sliding at the beam-column interface increases bond slip (and axial elongation) due to the degradation of the concrete-bar bond. Also, shear sliding stiffness is further reduced with an increase in bond slip. Hence, the interdependence between axial elongation and shear sliding is complex. This subsection, however, seeks to develop a simple formulation to quantify this interdependence.

Recalling that $\mu = \theta_m/\theta_y$, Equation (17) can be rewritten as:

$$\delta_{el} = \frac{\lambda}{2}\mu\theta_y\left(d - d'\right) \tag{28}$$

Rearranging Equation (28):

$$\mu = \frac{\delta_{el}}{0.5\lambda\theta_y\left(d - d'\right)} \tag{29}$$

Putting Equation (29) into Equation (26),

$$\Delta_{ss} = \Delta_{ss,y} \cdot \left(\frac{\delta_{el}}{0.5\lambda\theta_y\left(d - d'\right)}\right)^{a_2} \tag{30}$$

From the Opabola and Elwood[16] formulation for evaluating the yield rotation of RC beam-column components ($\theta_y = \beta\varepsilon_y a/2d$), and assuming $(d\text{-}d')/d$ equals 0.8, Equation (30) can be simplified as:

$$\Delta_{ss} = \Delta_{ss,y} \cdot \left(\frac{5\delta_{el}}{\lambda\beta\varepsilon_y a}\right)^{a_2} \tag{31}$$

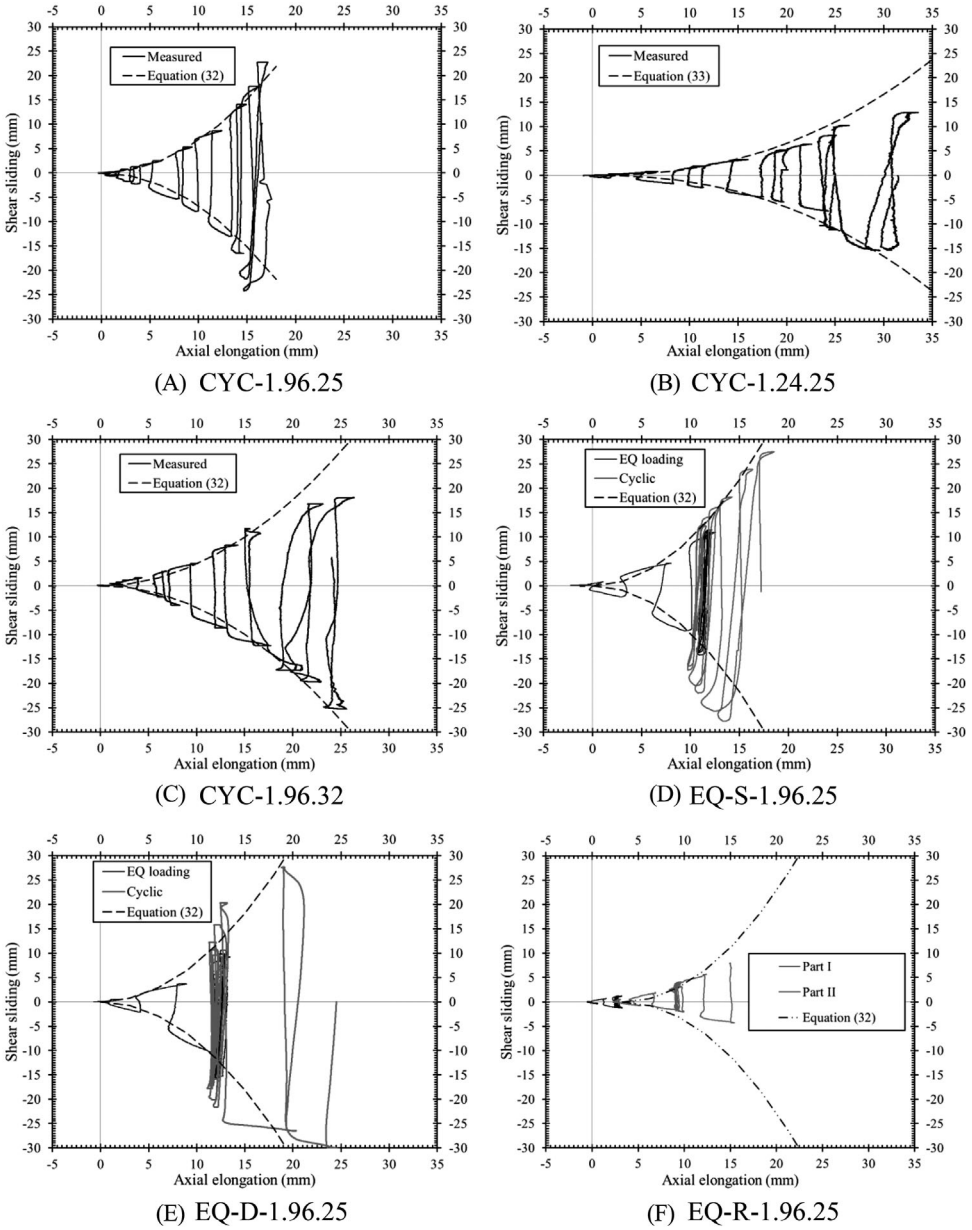

FIGURE 13 Relationship between axial elongation and shear sliding.

It is noted that δ_{el}/a is the axial strain in the beam; hence, from Equation (31), it can be concluded that the ratio of axial strain in the component to the yield strain of the longitudinal bar is quadratically proportional (assuming a_2 equals 2) to the magnitude of shear sliding displacement for slender beams. β is a coefficient that accounts for the contribution of bar slip and shear deformation to yield rotation, and it is expressed as a function of aspect ratio (See Opabola and Elwood[16])

For a beam with $a/d \geq 3$, a_2 equals 2 and if a single-crack plastic hinge behaviour is expected, $\lambda = 1.3$. Equation (31) can be approximately rewritten as:

$$\Delta_{ss} = \Delta_{ss,y} \cdot \left(\frac{4\delta_{el}}{\beta \varepsilon_y a} \right)^2 \tag{32}$$

As previously proposed, for the squat Specimen CYC-1.24.25, a λ of 2.0 and a_2 of 2.3 is adopted; such that from Equation (31),

$$\Delta_{ss} = \Delta_{ss,y} \cdot \left(\frac{2.5\delta_{el}}{\beta \varepsilon_y a} \right)^{2.3} \tag{33}$$

TABLE 3 Comparison of measured and predicted effective stiffness for all specimens.

Specimen	Measured EI_{eff}/EI_g	Predicted EI_{eff}/EI_g		Measured/Predicted	
		ASCE 41-17	Opabola and Elwood (2020)	ASCE 41-17	Opabola and Elwood (2020)
CYC-1.96.25	0.22	0.3	0.23	0.73	0.96
CYC-1.24.25	0.16	0.3	0.14	0.53	1.14
CYC-1.96.32	0.23	0.3	0.23	0.77	1.00
EQ-S-1.96.25	0.21	0.3	0.23	0.7	0.96
EQ-D-1.96.25	0.26	0.3	0.23	0.87	1.13
EQ-R-1.96.25	0.25	0.3	0.23	0.83	1.09

As shown in Figure 13B, Equation (33) provides a good estimate of the relationship between shear sliding and axial elongation for CYC-1.24.25. Additional testing is, however, required to further validate Equation (33) for squat beams.

8 | PREDICTION OF FORCE-DISPLACEMENT RESPONSE

8.1 | Effective stiffness

According to ASCE/SEI 41-17,[17] the effective stiffness (EI_{eff}) of a RC beam can be taken as 30% of the gross section (EI_g) of the beam. The measured effectiveness from each test specimen was derived from the measured yield displacement (as described previously) as:

$$EI_{eff} = \frac{V_{\max} a^3}{3\Delta_y} \tag{34}$$

where Δ_y is the measured yield displacement, V_{max} is the measured peak strength, a is the shear span of the specimen.

The measured effective stiffness for all six test specimens is presented in Table 3. A comparison of measured effective stiffness values for the beams to that predicted by ASCE/SEI 41-17 is presented in Table 3. As shown in Table 3, the effective stiffness of all specimens were all over-predicted.

The over-prediction of the effective stiffness by ASCE/SEI 41-17 is due to the fact that the effective stiffness provisions of ASCE/SEI 41-17 only account for flexural rigidity, neglecting the contribution of bar slip and shear deformation. In a recent study, Opabola and Elwood[16] proposed a formulation for accounting for the contribution of bar slip and shear deformation to effectiveness as function of the aspect ratio (a/d) of the component, such that:

$$\frac{EI_{eff}}{EI_g} = \alpha\left(0.27\left(\frac{a}{d}\right) - 0.07\right) \leq \alpha \tag{35}$$

where α is the flexural rigidity of the component and can be taken as proposed by ASCE/SEI 41-17. For a beam, α is taken as $0.3EI_g$.

A comparison of measured and predicted, using Equation (35), effective stiffness values for the beams is presented in Table 3. As shown in Table 3, the effective stiffness of all specimens are well-predicted. For specimen CYC-1.24.25 with a short aspect ratio, Equation (35) is able to adequately capture the lower stiffness in the specimen relative to the other slender beams. The higher measured effective stiffness of Specimen EQ-D-1.96.25, relative to the EQ-S-1.96.25 subjected to a pseudo-static loading rate, may be attributed to the higher strain rate. The effect of strain rate on the measured is, however, not so significant; hence, it is assumed that Equation (35) is applicable to components under dynamic strain rates.

8.2 | Plastic rotation capacity

Formulations presented in the preceding sections have been used to analyse the behaviour of components with single-crack plastic hinge behaviour. The interdependence and/or relationship between axial elongation, shear sliding

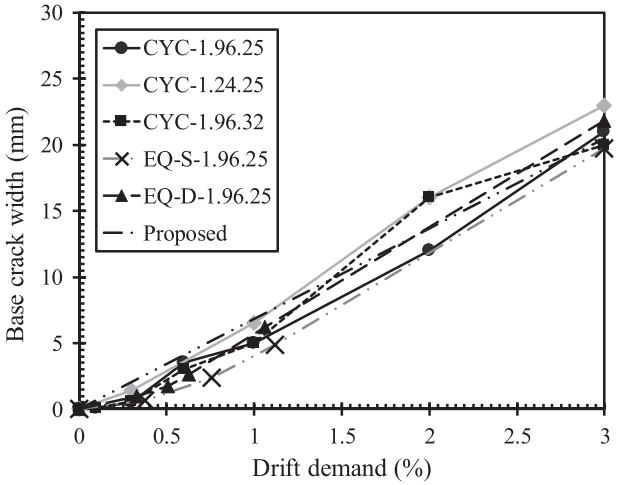

FIGURE 14 Adequacy of Equation (36) in predicting the relationship between maximum crack width at peak drift demand.

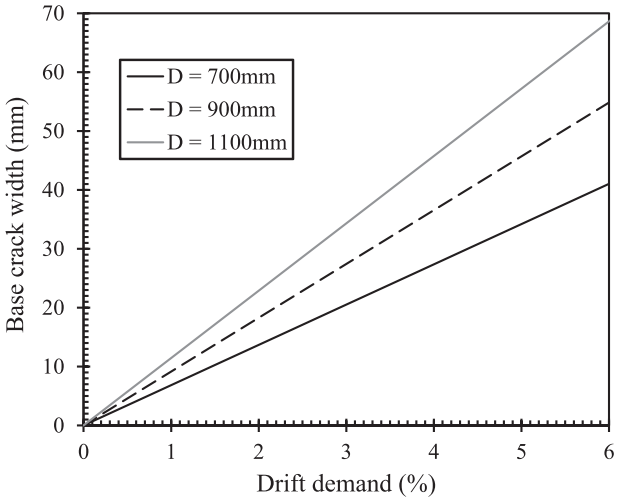

FIGURE 15 Influence of beam depth on base crack width at different drift demands, computed using Equation (36).

displacement and drift demand has been mathematically established. The mathematical formulations are considered applicable when rigorous predictions are desired. For most engineering applications (e.g. seismic assessment), however, assessing the deformation capacity of these beams is the main objective.

From Equations (14), (15) and (20), it can be easily derived that $\delta_2 = 0.13\delta_1$. Putting this back into Equation (14), this leads to:

$$\theta_m = \frac{0.87\delta_1}{d - d'} \tag{36}$$

The efficiency of Equation (36) in predicting the relationship between base crack width measured at the tensile end and drift demand is shown in Figure 14. Experimental data from test specimens suggest that the relationship between base crack width and drift demand can be assumed to be linear. Also, as shown in Figure 14, this linear relationship is well captured by Equation (36).

As shown in Equation (36), the relationship between base crack width and drift demand is influenced by the section depth. For section depths of 700 mm, 900 mm and 1200 mm, assuming the corresponding d—d' of 595 mm, 795 mm and 995 mm, respectively, the relationship is depicted in Figure 15. As shown in Figure 15, deeper beams are likely to have larger crack widths for a given drift demand. For example, a 3% drift demand corresponds to a crack width of approximately 20 mm and 35 mm in 700 mm and 1100 mm deep beams, respectively.

TABLE 4 Comparison of the adequacy of ASCE/SEI 41-17 and Equation (37) in estimating the plastic rotation capacity of the beams

Specimen	Measured θ_p (%)	Predicted θ_p (%)		Measured/Predicted	
		ASCE 41-17	Equation (37)	ASCE 41-17	Equation (37)
CYC-1.96.25	4.5	2.5	4.4	1.8	1.0
CYC-1.24.25	4.6	2.5	4.4	1.8	1.0
CYC-1.96.32	6.2	2.5	5.2	2.5	1.2

Thus, enough care must be taken to ensure the base crack width at an expected seismic drift demand on a beam with single-crack plastic hinge behaviour is acceptable for the spatial integrity of the frame system.

As mentioned earlier, the response of a beam with single-crack plastic hinge behaviour consists of three phases. The elastic response of such beams (i.e. contribution of different deformation components) is similar to that of a conventional beam. As shown in Table 3, the measured effective stiffness of the beams are well-predicted by formulations developed for components with distributed cracking. To predict the inelastic rotation capacity of beams with single-crack plastic hinge behaviour, it is suggested that the formulation for a pure-bond slip mechanism presented previously in this paper be modified to account for the influence of shear sliding deformation. As observed in the beam specimens, once high tensile strains developed in the longitudinal bars, they became susceptible to bar buckling during a load reversal due to the combined effect of lateral dowel forces and longitudinal compression forces. To account for this, as recommended by Priestley and Kowalsky,[18] it is suggested that the ultimate tensile strain capacity of the longitudinal reinforcement be limited to 0.06. Excessive longitudinal bar buckling may be expected once this strain limit is exceeded. It is noted that this tensile strain limit applies to beams with stirrup spacing $s \leq 3 + 6(f_u/f_y - 1)d_b$.[12] A lower strain limit may be adopted if the stirrup spacing is larger.

Hence, the plastic rotation capacity of a beam with a single-crack plastic hinge mechanism can be estimated from Equation (13), assuming an ultimate tensile strain capacity of 0.06 and taking d—c to be equal to 0.8D, as:

$$\theta_p = \frac{0.15 l_{sp}}{D} \tag{37}$$

Where l_{sp} can be estimated from Equation (11).

The adequacies of Equation (37) and ASCE/SEI 41-17 provisions are presented in Table 4. ASCE/SEI 41-17 provides an estimate for the plastic rotation capacity at onset of loss of lateral strength for flexure-dominated beams as a function of maximum shear stress, longitudinal and transverse reinforcement detailing. The maximum shear stresses ($V_u/(bd\sqrt{f'_c})$) of Specimens CYC-1.96.25, CYC-1.96.32 and CYC-1.24.25 are $0.17\sqrt{f'_c}$, $0.22\sqrt{f'_c}$ and $0.26\sqrt{f'_c}$ respectively; hence the predicted plastic rotation at capacity at the onset of loss of lateral resistance for all three specimens equals 0.025.

Recall that the measured ultimate drift capacity was defined as a 20% loss in lateral resistance. The measured plastic rotation capacities at the onset of loss of lateral strength of the test specimens were evaluated as the difference between measured drift capacities and the yield rotation which was measured as previously described in this paper.

As shown in Table 4, ASCE/SEI 41-17 underestimates the plastic rotation capacities at the onset of loss of lateral resistance for all three specimens. On the other hand, Equation (37) provides a good estimate of the plastic rotation capacities. It is, therefore, proposed that Equation (37) be adopted for predicting the plastic rotation capacity of modern beams susceptible to single-crack plastic hinge behaviour.

Looking at Table 4, the deformation capacity of Specimen CYC-1.24.25 was well-predicted by Equation (37) despite the fact that the response of Specimen CYC-1.24.25 was not dominated by a single-crack. This suggests that Equation (37) may be applicable for evaluating the drift capacity of ductile RC beams. may be applicable for evaluating the drift capacity of ductile conventional RC beams with distributed cracking. Further studies are required to validate this.

The seismic assessment procedure for a beam susceptible to single-crack plastic hinge behaviour would entail:

1. Evaluation of the probable peak shear stress demand ($V_u/(bd\sqrt{f'_c})$) of the beam. If $V_u/(bd\sqrt{f'_c}) \geq 0.25\sqrt{f'_c}$, assume that distributed shear cracking is likely; else, assume that the response of the beam would be dominated by a single-crack plastic hinge behaviour.
2. Evaluation of the probable yield rotation using the Opabola and Elwood[16] formulation.
3. Evaluation of the probable plastic rotation capacity using Equation (37) and summing up the computed yield rotation and plastic rotation capacity to derive the drift capacity limit of the beam

4. Evaluation of expected beam elongation at the predicted drift capacity using Equation (17). If $V_u/(bd\sqrt{f'_c}) \geq 0.25\sqrt{f'_c}$, $\lambda = 2.0$; else, $\lambda = 1.3$.
5. Evaluation of the expected shear sliding deformation using Equation (31).
6. If the computed shear sliding and axial elongation deformations are deemed unacceptable based on deformation compatibility considerations or any engineering requirement, the deformation capacity from step 3 should be reduced until a target shear sliding or axial elongation deformation is achieved.

The presented experimental data and formulation are based on unrestrained beams. Slab effect and frame actions may induce axial restraint in typical frame beams. Additional testing is needed to validate the proposed formulations for restrained beams.

9 | CONCLUSION

Due to bar curtailment at the column face, certain modern beams (i.e., designed according to modern seismic design philosophy) may be susceptible to a single-crack plastic hinge behaviour instead of the desirable conventional distributed cracking mechanism. The response of beams with single-crack plastic hinge behaviour is different from that with distributed plastic hinge behaviour. This study explores the response of beams with single-crack plastic hinge behaviour due to curtailed longitudinal bars using experimental data from six full-scale beam test specimens.

Experimental results from the six specimens show that the inelastic response of such a beam is dominated by the fixed-end rotation mechanism via bond-slip. Due to reinforcement and geometrical detailing, however, there might be variations in the response of the beams expected to be dominated by single-crack plastic hinge behaviour. Due to high shear stress, beams with or without curtailed bars having $V_u/(bd\sqrt{f'_c}) \geq 0.25\sqrt{f'_c}$ should be expected be have significant diagonal cracking along the shear span.

In beams dominated by single-crack plastic hinge behaviour due to curtailed longitudinal bars, once flexural yielding occurs at the beam-column interface and inelastic deformations starts concentrating at the interface, shear forces can only be transmitted across the crack by two modes—aggregate interlock between the surfaces of the crack and dowel action in the reinforcement crossing the crack. As the beam elongates, aggregate interlock is lost and dowel resistance serves as the only shear resisting mechanism. This results in an increase in shear sliding deformation. Hence, the response of beams with single-crack plastic hinge behaviour is characterised by the interdependence between base shear sliding and axial elongation as displacement demand increases. This relationship was derived analytically and validated using experimental results. Also, it was concluded that beams with single-crack plastic hinge behaviour may experience half of the axial elongation expected in beams with distributed cracking. However, due to a higher likelihood of diagonal cracking initiation along shear span, short beams with curtailed bars ($a/d \leq 2$) or $V_u/(bd\sqrt{f'_c}) \geq 0.25\sqrt{f'_c}$ should be treated as if distributed cracking is expected.

Also, procedure for seismic assessment of such beams is proposed. The proposed formulations can be adopted in developing adequate numerical models for simulating the response of RC frames with beams susceptible to single-crack response due to curtailed longitudinal bars.

A limitation of this study is the unavailability of an extensive experimental dataset to validate the proposed formulations. Additional testing on beams susceptible to distributed plastic hinge behaviour is required to validate this study further. Furthermore, the presented experimental data and formulation are based on unrestrained beams. Slab effect and frame actions may induce axial restraint in typical frame beams. Additional testing is needed to validate the proposed formulations for restrained beams.

ACKNOWLEDGEMENTS

The experimental program was supported by QuakeCoRE. The first author would also like to acknowledge the United Kingdom Research and Innovation (UKRI) funding [project reference EP/X023710/1] which supported the analytical study.

DATA AVAILABILITY STATEMENT

The data that support the findings of this study are available from the corresponding author upon reasonable request.

REFERENCES

1. Kam WY, Pampanin S, Elwood K. Seismic performance of reinforced concrete buildings in the 22 February Christchurch (Lyttelton) earthquake. *Bull N Z Soc Earthq Eng*. 2011;44(4):239-278.
2. Henry RS. Assessment of minimum vertical reinforcement limits for RC walls. *Bull N Z Soc Earthq Eng*. 2013;46(2):88-96.
3. Opabola EA, Elwood KJ. Seismic performance of reinforced concrete beams susceptible to single-crack plastic hinge behavior. *J Struct Eng*. 2023 149(4).
4. Choi Y, Chao S-H. Balanced damage concept for beam-to-column connections of special moment frames using HPFRC. *ACI Struct J*. 2019;116(1):237.
5. Mander JB, Rodgers GW, Analysis of low cycle fatigue effects on structures due to the 2010–2011 Canterbury Earthquake Sequence. Proceedings of the Tenth Pacific Conference on Earthquake Engineering (PCEE). Sydney, 2015.
6. MBIE., EQC., NZSEE., et al. Part C5, Concrete buildings, Technical Guidelines for Engineering Assessment Guidelines. 2017.
7. Standards New Zealand. NZS 3101:1982, Code of Practice for Design of Concrete Structures. 1982.
8. Standards New Zealand. NZS 3101:2006:A3 – Concrete structures standard. Wellington, NZ, 2006, 1-698 pp.
9. Bertero VV, Popov EP. *Hysteretic behavior of ductile moment-resisting reinforced concrete frame components*. College of Engineering, University of California; 1975.
10. Sezen H, Setzler EJ. Reinforcement slip in reinforced concrete columns. *ACI Struct J*. 2008;105(3):280-289.
11. Paulay T, Priestley MJN, Seismic Design of Reinforced Concrete and Masonry Buildings. 1992, 765 pp.
12. Priestley MJN, Calvi GM, Kowalsky MJ. *Displacement – based seismic design of structures*. IUSS Press; 2007:597.
13. Fenwick RC, Megget LM. Elongation and load deflection characteristics of reinforced concrete members containing plastic hinges. *Bull N Z Soc Earthq Eng*. 1993;26(1):28-41.
14. Sarrafzadeh M. *Determination of a reparability limit state for concrete structures impacted by earthquake damage*. University of Auckland; 2020. PhD thesis.
15. Elwood KJ, Eberhard MO. Effective stiffness of reinforced concrete columns. *ACI Struct J*. 2009;106(4):476-484.
16. Opabola EA, Elwood KJ. Simplified approaches for estimating yield rotation of reinforced concrete beam-column components. *ACI Struct J*. 2020;117(4):279-291.
17. ASCE. *Seismic evaluation and retrofit of existing buildings: ASCE/SEI 41-17*. American Society of Civil Engineers; 2017, 550 pp.
18. Priestley MJN, Kowalsky MJ. Aspects of drift and ductility capacity of rectangular cantiliver structural walls. *Bull NZ Natl Soc Earthq Eng*. 1998;31(December):73-85.

How to cite this article: Opabola EA, Elwood KJ. Flexure-axial-shear interaction of ductile beams with single-crack plastic hinge behaviour. *Earthquake Engng Struct Dyn*. 2023;1-20. https://doi.org/10.1002/eqe.3873